Title
The effects of high energy deuteron ion beam irradiation on the tensile behavior of HT-9

Authors
Stevenson, Sarah
Dong, Andrew
Xie, Yujun
et al.

Publication Date
2022-11-01

DOI
10.1016/j.nimb.2022.09.001

Peer reviewed

Nuclear Instruments and Methods in Physics Research B 531 (2022) 65–73

Contents lists available at ScienceDirect

Nuclear Inst. and Methods in Physics Research, B

journal homepage: www.elsevier.com/locate/nimb

The effects of high energy deuteron ion beam irradiation on the tensile behavior of HT-9

Sarah Stevenson [a,*], Andrew Dong [a], Yujun Xie [a], Jon Morrell [a], Andrew S. Voyles [a], Jeff Bickel [a], Lee Bernstein [a,b], S.A. Maloy [c], Peter Hosemann [a,b]

[a] Department of Nuclear Engineering, University of California Berkeley, Berkeley, USA
[b] Lawrence Berkeley National Laboratory, Berkeley, USA
[c] Pacific Northwest National Laboratory, Richland, WA, USA

ARTICLE INFO

Keywords:
Deuteron irradiation
Tensile testing
Radiation damage
HT-9
Size effects

ABSTRACT

Ion beam implantations are widely performed to understand the effects of irradiation-induced displacement damage on nuclear structural materials. However, the volume of material that can be investigated is often limited by the maximum energies of accelerator facilitates, leading to a limitation in the thickness of samples whose mechanical properties can be evaluated. The Lawrence Berkeley National Laboratory's 88-Inch Cyclotron offers a wide range of ions and energies, allowing for material ion implantations at larger scales than typical. Four HT-9 SS-J-geometry tensile specimens were polished and then irradiated with deuterons at the 88-Inch Cyclotron to doses of approximately 0.2 dpa prior to small scale tensile testing. The results from this study show irradiation hardening characterized by the tensile test results and black dot irradiation defects. Additionally, a comprehensive look at low temperature irradiations of high-Cr F/M steels is presented and our results show agreement with the available data.

1. Introduction

Radiation damage can significantly change the mechanical properties of materials. In ferritic/martensitic (F/M) steels, low temperature ($\leq$300 °C) radiation-induced displacement damage has been known to cause hardening which is characterized by an increase in yield and ultimate tensile strength and a decrease in uniform elongation (ductility) [1–9]. The reliability of materials in nuclear environments is still an outstanding concern, prompting efforts to develop new "radiation tolerant" materials or enhance the confidence in existing ones. The fidelity and reliability of mechanical testing is similarly of interest, given the rising popularity of smaller length scale testing [10,11].

Traditionally, reactors or accelerators are used to irradiate materials for performance testing [1–9,12]. Both approaches benefit from smaller material testing techniques. Small scale testing produces a smaller volume of radioactive-material and requires a shorter irradiation time to achieve a desired number of displacements per atom (dpa), leading to faster testing throughput, reduced radiation safety concerns, and facilitating sample testing with low-energy accelerators. Limited space in irradiation facilities and the rapidly growing availability of new alloys are additional driving forces for small scale testing [10]. Today, many small-scale testing techniques, such as nanoindentation, microcompression, microtensile, and microbend testing, have been adapted for nuclear applications. However, a significant amount of research is still needed to correlate small-scale testing with bulk properties [13].

The 88-Inch Cyclotron shows promise for future macroscale materials testing, offering a broad range of heavy and light ions ($Z \leq 92$), high energies ($K = 140$) necessary to penetrate through macroscale samples, and high currents (10's of p-μA) for achieving at least 1 dpa in several days of irradiation time. This work demonstrates a quick-turnaround material testing capability using the Cyclotron and benchtop tensile testing of irradiated samples, contributes to the growing F/M steel property database, and provides insight into irradiation damage effects and small-scale testing limitations.

2. Material and methods

In this study, SS-J tensile geometries with different thicknesses were irradiated with high-energy deuterons and subsequently tested. The thickness range of this study, combined with concurrent size effect

* Corresponding author.
E-mail addresses: srstevenson@berkeley.edu (S. Stevenson), peterh@berkeley.edu (P. Hosemann).

https://doi.org/10.1016/j.nimb.2022.09.001
Received 23 September 2021; Received in revised form 30 August 2022; Accepted 1 September 2022
Available online 7 October 2022

studies, was selected to bridge the experimental length-scale gap and make use of the irradiation depths possible with the 88-Inch Cyclotron at Berkeley [3]. HT-9 was used since it is a candidate material for advanced nuclear reactors with an extensive tensile testing database [2,5,14].

HT-9 SS-J tensile specimens were prepared from heat # V1608621 produced by Metalwerks with a composition of Fe 12.2Cr-1.1Mo-0.51 W-0.57Ni-0.30 V-0.21C-0.29Si-0.32Mn (in wt%). The stock HT-9 was heat treated at 1040 °C for 30 min, AC and subsequent 760 °C for 1 hr, AC. After the heat treatment, the stock was cut into a bar with SS-J outer dimensions using wire electrical discharge machining (EDM). The outside of the SS-J bar was polished to remove an oxide scale. A Struers Accutom-50 with a SiC blade was used to slice individual tensile specimens from the larger SS-J bar. Subsequently, the tensile samples were polished down to thickness using SiC abrasive sheets up to 1200/P4000 grit, and optically inspected to ensure a clean and defect-free surface. The thickness of each sample was measured at each shoulder and gauge length using a micrometer with ±1 μm tolerance.

2.1. Deuteron irradiation

The 33 MeV deuteron irradiation was carried out at the Lawrence Berkeley National Laboratory's 88-Inch Cyclotron. During the 5.3-day irradiation, the current fluctuated from 9 μA to 1 μA, with a weighted average current of about 3.9 μA, corresponding to about 3×10^{18} ions. The deuterons were incident on a target stack with 4 tensile specimens, as depicted in Fig. 1(a) [15]. Due to the high energies used, there were concerns with the sample clamping configuration providing good thermal contact for efficient sample cooling. Thus, two different sample clamping configurations (side-by-side and back-to-back) were used to assess the effectiveness of each and set a precedent for future experimental configurations. The 202 μm and 91 μm thin samples were stacked on top of each other and clamped between two 1.45 mm thick sheets of Be metal. The remaining two samples, each 40 μm thin, were placed side-by-side and clamped between one of the 1.45 mm sheets of Be and the Al beam stop. The sample temperature was not monitored during the irradiation. However, the samples were placed in good thermal contact with a continuous flow low conductivity water cooling plate, and previous 5-day high powered irradiations with this configuration had a steady state sample temperature under 60 °C [16].

In addition to the deuteron beam, secondary neutrons were produced from the (d,n) reaction in Be. To measure the neutron fluence and energy, 1 cm diameter by 1 mm thick Ni and Yt neutron monitor foils were placed in a ½-inch diameter blind hole in the back of the beam stop. Following the experiment, the neutron monitor foils were counted on an ORTEC GMX Series (model GMX-50220-S) High-Purity Germanium (HPGe) detector, and calibrated with 1 μCi Ba-133, Cs-137 and Eu-152 sources from Eckert & Ziegler, traceable to NIST. Using the ^{58}Ni(n,2n)^{57}Ni, ^{58}Ni(n,p)^{58}Co, ^{89}Y(n,2n)^{88}Y, and ^{89}Y(n,3n)^{87}Y monitor reactions and cross sections from the IRDFF-II Library, the secondary neutron fluence incident on the samples was calculated to be $(2.83 \pm 0.19) \times 10^{17}$ neutrons/cm^2, with an average neutron energy of 11.87 MeV [17].

The spatial profile of the deuteron beam entering the target stack was imaged with Radiochromic film (Gafchromic EBT3). Fig. 1(b)–(d) shows the location and shape of the beam, with the SS-J geometries included for scale. The beam spot size was approximately 0.38 cm^2 and centred on the gauge regions to avoid irradiating the sample grippers. The 33 MeV deuteron beam was degraded by the layers of Be and HT-9 samples in the target stack. Energy loss calculations were performed by using a cumulative trapezoidal integration of the stopping curves produced by SRIM-2013 with 40 eV displacement energy, resulting in a 25.6 MeV, 21.8 MeV, and 19.4 MeV beam incident on the 202 μm, 91 μm, and 40 μm samples, respectively [18]. Consequently, all the samples, save for the two side-by-side 40 μm samples, were expected to receive energy-dependent doses. The deuteron dose in each sample was also calculated using the SRIM-2013 code. Fig. 2 shows the calculated dpa as a function of depth for the samples. The average SRIM-calculated dpa in the 202 μm, 91 μm, and 40 μm samples was 0.18, 0.2, and 0.22, respectfully. It should be noted that the additional secondary neutron fluence contributed to the observed sample radioactivity and increased dpa relative to that calculated using SRIM.

Approximately 5 months following the irradiation, activation product activities in the tensile samples were measured through gamma spectroscopy [19]. To avoid saturating the HPGe detector, the samples were placed in a lead pig approximately 2 m from the detector's front face. All tensile samples were counted together, and the resulting spectrum is shown in Fig. 3. The overwhelming majority of the produced activity was due to ^{56}Co (approximately 98.6 mCi), which masked other expected spectral lines, such as those from ^{58}Co and ^{60}Co. ^{56}Co has a half-life of 77.236 ± 0.026 days [20], permitting an estimate of the activity at the end of irradiation of 394.4 mCi of ^{56}Co.

From the bulk Fe content of HT-9 steel, ^{56}Co is produced from ^{56}Fe (d,2n) (threshold: 7.8 MeV), ^{57}Fe(d,3n) (threshold: 15.7 MeV), and a small amount via ^{58}Fe(d,4n) (threshold: 26 MeV) [21]. Production off

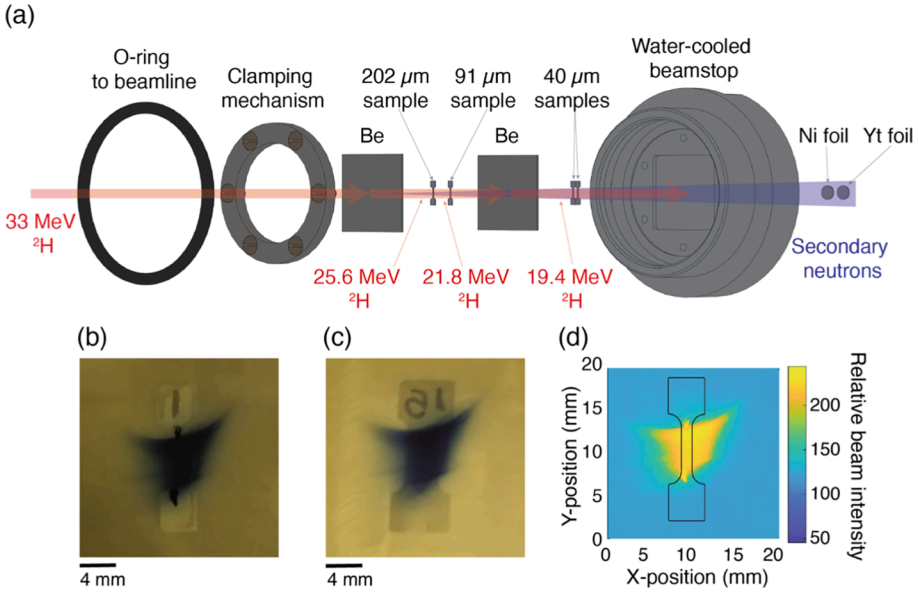

Fig. 1. Experimental setup of the 5.3 day HT-9 SS-J deuteron irradiation at the 88-inch Cyclotron. (a) Exploded view of the target setup. The 33 MeV deuterons (^{2}H) were attenuated by the Be and HT-9 layers, and the deuteron breakup on the Be produced secondary neutrons which were monitored with Ni and Yt foils. (b) Photo of the deuteron beam intensity profile measured with Radiochromic film on the 202 and 91 μm sample stack. (c) Photo of the deuteron beam intensity profile measured with Radiochromic film on the 40 μm samples. (d) Radiochromic film measurement result with an overlay of the SS-J geometry. As shown in (b)–(d), the beam spot was ~0.38 cm^2 and centred on the SS-J gauge region so the grip sections were not irradiated.

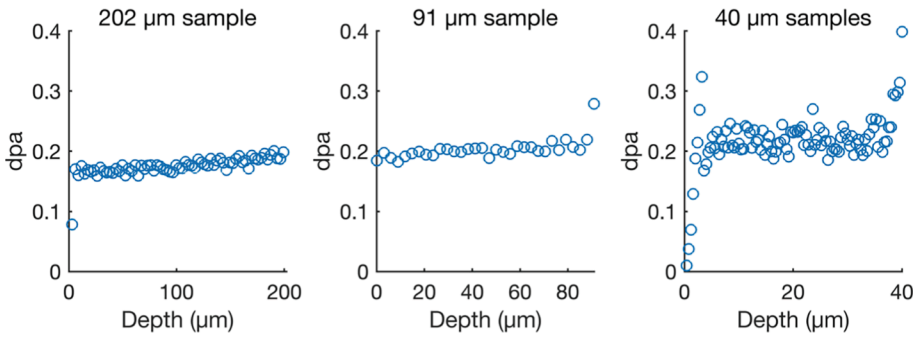

Fig. 2. Dpa as a function of depth into the HT-9 samples, calculated from SRIM-2013 code. The average dpa was 0.18, 0.2, and 0.22 for the 202 μm, 91 μm, and 40 μm samples, respectively.

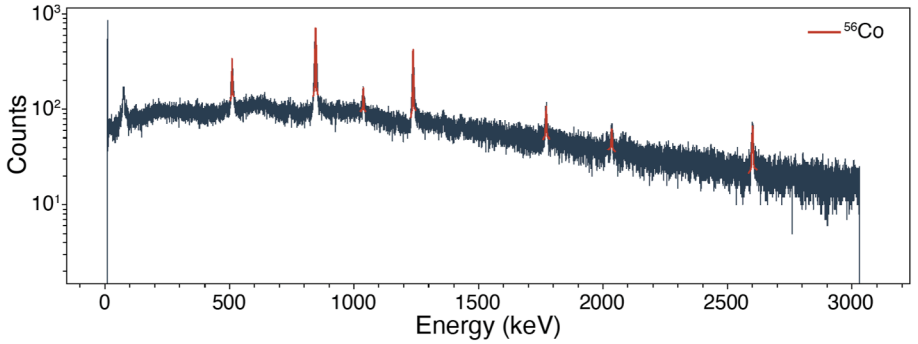

Fig. 3. Gamma spectrum from all four HT-9 SS-J samples measured 5 months following the 33 MeV deuteron irradiatuon. The samples were counted in a lead pig 2 m away from the front of the HPGe detector. The majority of the measured radioactivity was from ^{56}Co, whose photopeaks are indicated in red. (For interpretation of the references to colour in this figure legend, the reader is referred to the web version of this article.)

the W and Mo content is not energetically possible with 33 MeV deuterons. However, the ^{56}Co can be made in great quantities via ^{58}Ni(d, a)^{56}Co (no threshold), ^{60}Ni(d,a2n) (threshold: 14.3 MeV) and ^{61}Ni(d, a3n) (threshold: 22.4 MeV). In addition, rather than emitting an alpha particle, each of those Ni(d,ax) channels can instead emit combinations of two protons and two neutrons (at slightly higher energies), further boosting yields.

The samples were received at UC Berkeley for tensile testing approximately 8 months following the irradiation, to allow time for the Co activities to decay to a safe level for handling. The on-contact dose rate of each sample was measured using a calibrated ion chamber at the time of tensile testing. For the 202 μm, 91 μm, and two 40 μm samples, the on-contact dose rates at time of tensile testing were approximately 2 R/hr, 1 R/hr, 7 mR/hr, and 2 mR/hr, respectively. These dose rates made it acceptable to perform the tensile testing on a shielded benchtop.

2.2. Tensile testing

Tensile testing of both unirradiated and irradiated samples was carried out using a Kammrath & Weiss Tensile Module (KW) with a 500 N load cell and engineering strain rate of 3×10^{-3} /s (15 μm/sec stroke rate). Samples >600 μm thick required use of a 5 kN load cell. All samples were pulled until failure. An optical camera was employed to record a video of the samples during tensile testing, with the added ability to perform digital image correlation as needed. The original gauge thickness measured before testing was used for calculating the stress/strain curves and the machine compliance was subtracted from the load/displacement curves. These curves were used to determine 0.5% offset yield strength (YS), ultimate tensile strength (UTS), and reduced uniform elongation (UE). The UE is calculated by subtracting the elastic portion of the strain at UTS, whereas total uniform elongation would this portion.

2.3. Microscopy

After irradiation and tensile testing, the failure surface of each sample was characterized by Scanning Electron Microscopy (SEM) using a FEI Quanta 3D FEG. Then, the 40 μm sample with an on-contact dose rate of 7 mR/hr was taken as the representative sample for additional microstructure characterization. TEM lamella was lifted out from the irradiated gauge section, reasonably far from the fracture site, using a Thermo Scientific Scios 2 DualBeam focused ion beam system. The final lamella thickness after Ga ion beam thinning was approximately 108 nm. For the irradiated microstructure characterization, TEM images were acquired using a FEI ThemIS 60–300 STEM/TEM.

3. Results

Unirradiated HT-9 SS-J samples with gauge thicknesses ranging from 24 μm to 752 μm were used as controls for comparison of combined geometric and radiation effects on tensile properties. Supplementary Table 1 provides the irradiated and unirradiated samples' gauge thicknesses, YS, UTS, and UE, as well as the irradiated samples' dpa and on-contact dose rates.

The change in tensile properties are presented by stress–strain curves shown in the lefthand column of Fig. 4. Except for the 202 μm sample, which showed an increase in YS of approximately 15%, the average increase in YS after irradiation is approximately 35%. The difference in the 202 μm sample could have been due to premature fracture observed at the sample shoulder during the tensile testing. For all samples, compared to the unirradiated HT-9, the irradiated HT-9 undergoes significantly less strain hardening before fracture. A significant (approximately 75%) loss of ductility is observed with irradiation. It should be noted that since the irradiation utilized protons, hydrogen embrittlement needs to be considered. However, given that the ion beam

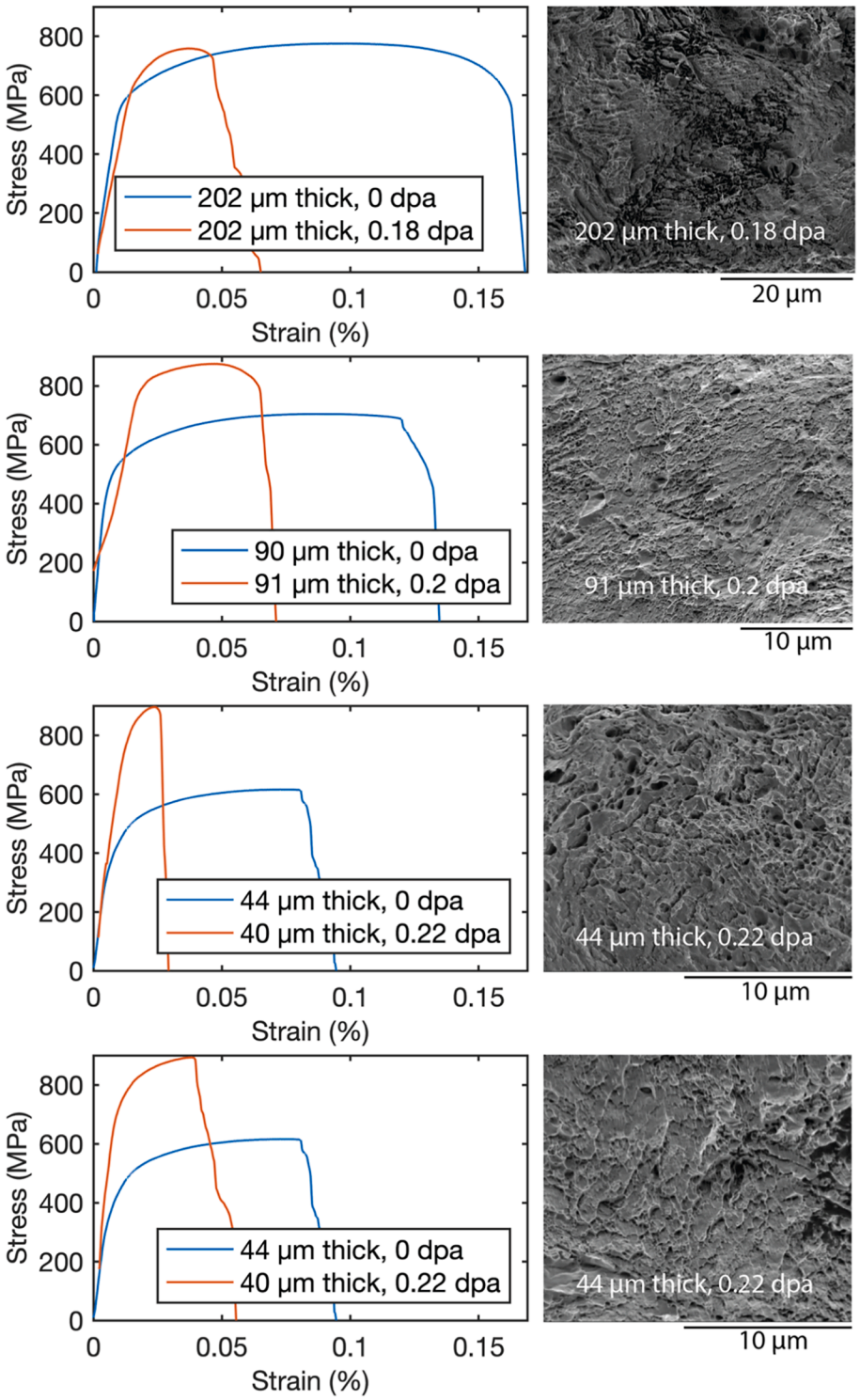

Fig. 4. Effect of 0.18, 0.2, and 0.22 dpa deuteron irradiation on the stress strain curve production of 202 μm, ~90 μm, and ~40 μm thick HT-9 SS-J tensile samples, respectively. An increase in YS and reduction in ductility is observed, indicating radiation hardening. Corresponding SEM images of the failure surfaces for are shown on the right, showing an intermediate ductile/brittle failure mechanism.

does not stop in the samples, hydrogen is highly mobile in metals, and the prolonged irradiation time, we would suggest that it the hydrogen is not a major concern during this irradiation. Ductility loss can be explained by radiation-induced displacement damage which clusters into cavities and loops. This displacement damage impedes dislocation motion during plastic deformation, thereby impacting YS and decreasing plasticity. A decrease in plasticity is expected to increase with dose, but eventually saturate when defect overlapping becomes dominant, which is often reported to be ~10 dpa for high-Cr F/M steels such as HT-9 [2,4,11,22].

Respective SEM micrographs of the failure surface for each irradiated sample is shown to the right of each stress–strain curve in Fig. 4. For all samples, the failure surface appears to be indicative of an intermediate ductile/brittle fracture mechanism. That is, the failure surfaces do not consist of entirely “dimpled” ductile type failure or “faceted” brittle type failure. HT-9 has a BCC crystal structure and therefore no close-packed

planes to allow for easy dislocation migration under mechanical deformation. BCC slip systems must be thermally activated, in what is known as the ductile–brittle transition temperature (DBTT). Although the DBTT of unirradiated HT-9 is below room temperature, radiation-induced upshifts in DBTT have been reported, meaning brittle failure is apparent at higher temperatures than it would be before irradiation, due to radiation hardening and/or radiation-induced segregation (RIS) of impurities to grain boundaries [2,4]. It is possible the moderate dose in this experiment has not shifted the DBTT enough, hence the appearance of an intermediate mode failure. Further, it should be noted that sample geometry effects on the failure mode are not decoupled from irradiation effects in this experiment.

To investigate the defect structure, the 40 μm thick, 7 mR/hr sample was characterized by TEM. Fig. 5(a) was produced using a two-beam condition, and shows the sample is heavily decorated with black dot irradiation defects. This expected based on previous neutron irradiations of HT-9, which show black dot defects at a small threshold dose, and resolvable loops beginning around 1 dpa [23,24]. An attempt was made to analyse the black dot defects, as demonstrated in Fig. 5(b)–(c), however, due to the low resolution, there is a significant error in quantifying the defects. Fig. 5(c) represents a high estimate of the defect size and number, while Fig. 5(d) represents a low estimate. As a result, the average major diameter of the black dots were approximately 6 ± 2 nm, and the number density is estimated $1.6 \times 10^{14} \pm 10^{14}$ m^{-2}.

Fig. 6 shows the obtained YS, UTS, and UE as a function of gauge thickness for unirradiated and the deuteron-irradiated samples. For the unirradiated (0 dpa) HT-9, the YS appears to remain relatively constant (~575 MPa) at thicknesses down to about 200 μm. Below 200 μm, the unirradiated YS values begin to decrease with a slope of approximately 0.9 MPa/μm. A similar trend is observed for the unirradiated UTS, with

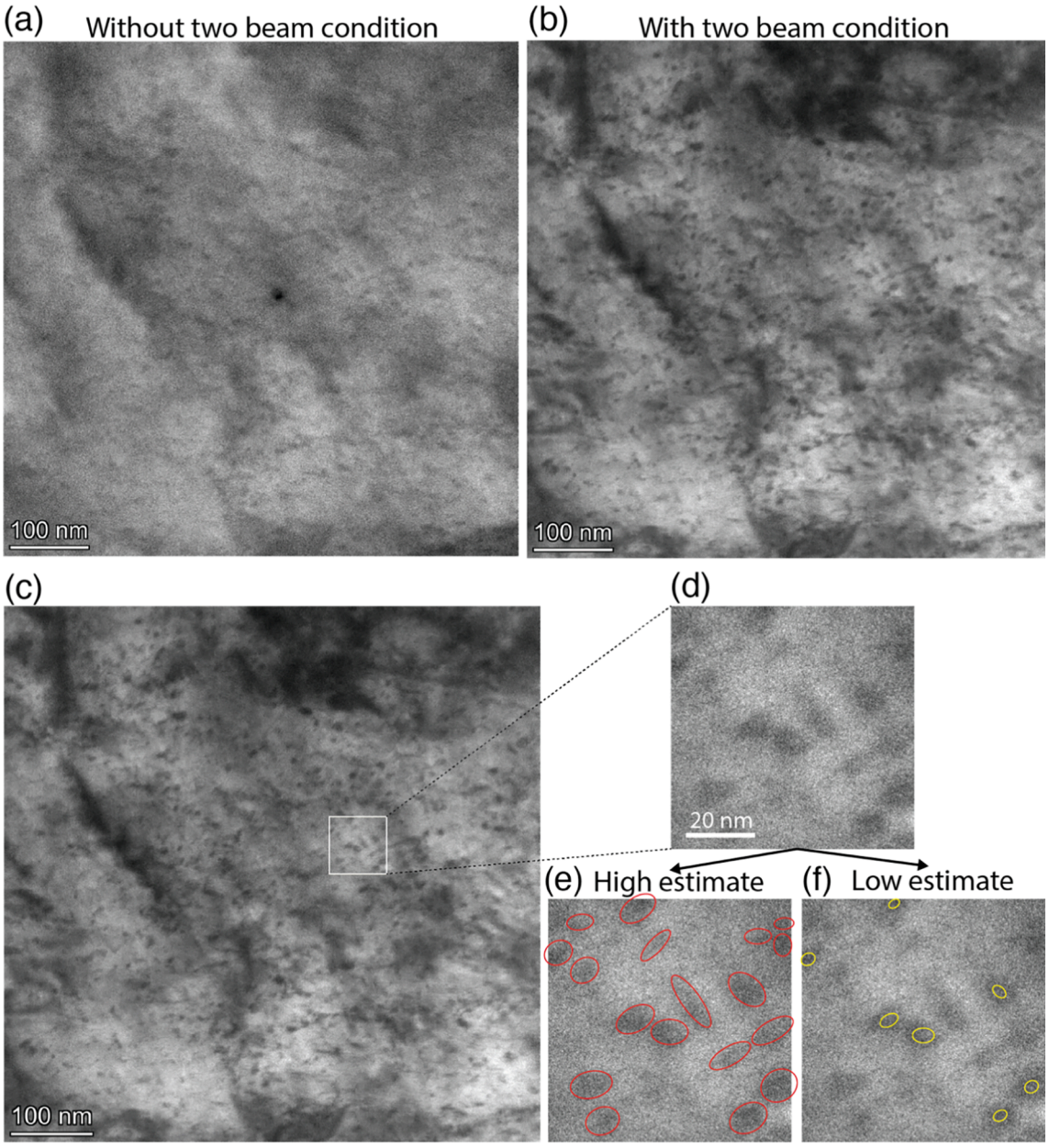

Fig. 5. TEM investigation of the 40 μm thick, 7 mR/hr sample. The TEM lamella was taken from the irradiated gauge section and far from the tensile fracture site. (a)–(b) A comparison of the same region without two beam and with two beam conditions, Black dot irradiation defects are revealed by the two beam condition. (c) Annotated version of (b), used in (d)–(f) to exemplify the method used to quantify the black dot defects. (d) Magnified area, annotated in (e),(f) as an example of a high and low estimate for the black dot radiation defect size and number.

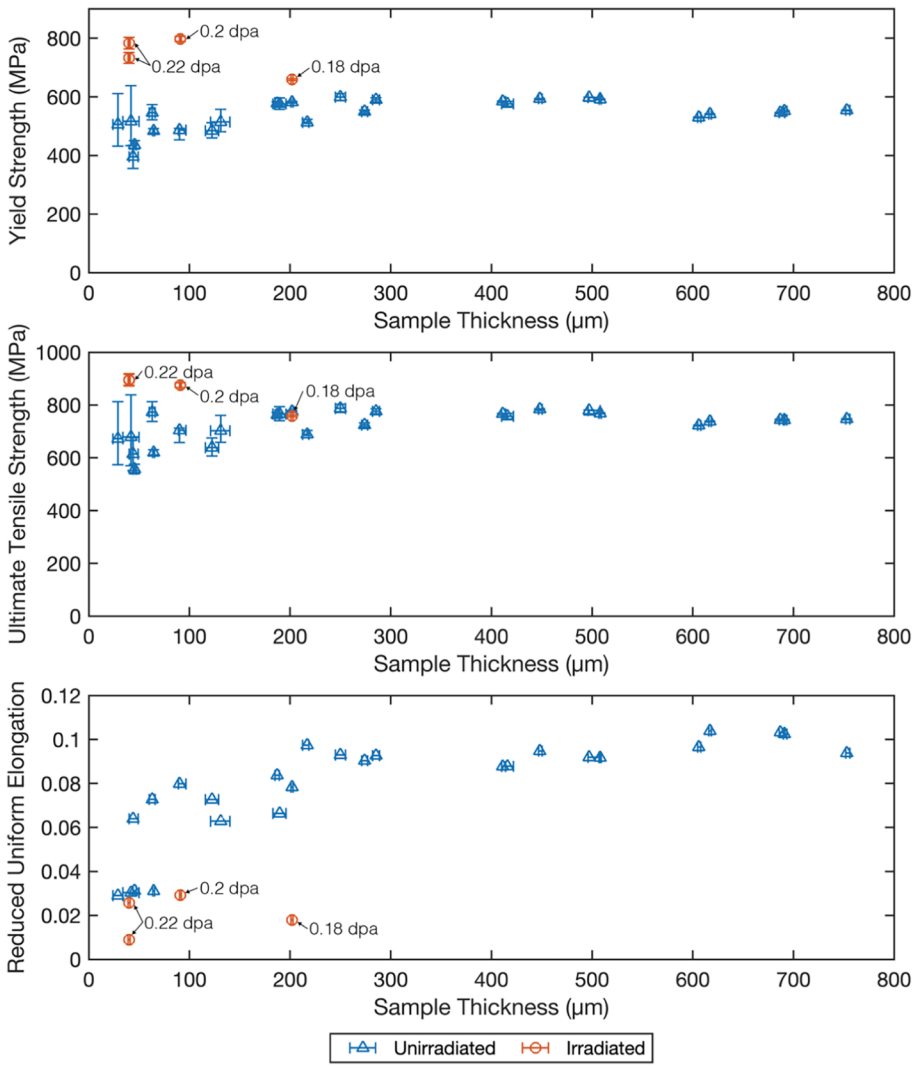

Fig. 6. Effects of 0.18–0.22 dpa deuteron irradiation on thickness dependence of YS, UTS, and UE in HT-9. Unirradiated data is adapted from Dong et al. [14]. A dip is observed below approximately 200 μm in all material properties for the unirradiated samples. The irradiated samples appear to show an increased YS and UTS and decreased UE compared to the unirradiated bulk (>200 μm) properties.

the UTS relatively constant (~750 MPa) then decreasing with a slope of about 1 MPa/μm below 200 μm. The unirradiated UE is also relatively constant (~0.09) then decreases with respect to gauge thicknesses below 200 μm, though when compared to that seen for YS and UTS, the dip is more significant. Around 50 μm, a ~70 % reduction in UE compared to bulk thickness is observed. The four irradiated samples with gauge thicknesses of 202, 91, and 40 μm exhibited a YS and UTS generally higher than that of the bulk (>200 μm) unirradiated values, UE generally lower than all unirradiated values, and these irradiated tensile properties did not increase with decreasing sample gauge thickness.

The small specimen preparation and tensile testing procedures used here are very repeatable. However, there is clear variance within the data, especially at thinner thicknesses. This variance may be due to limitations of the SS-J sample geometry at thicknesses much thinner than the design. Additionally, while thickness errors were calculated and plotted, the errors themselves are not comprehensive, and thickness variations on the order of ±5 μm may be increasingly significant with decreasing sample thickness. For the irradiated data, there are additional unaccounted for errors within the dpa calculations themselves, given the assumptions provided in the methods above and the differences in measured on-contact dose rates. For a more comprehensive explanation of scatter within the unirradiated data, the authors recommend reference [14].

The dependencies of some tensile properties such as YS on sample thickness and aspect ratio have previously been reported [25,26]. So long as the aspect ratio is not too extreme, the critical sample thickness can be attributed to sample microstructure; generally, about 10 grain diameters across the thickness is desired for reliable F/M steel tensile testing [24]. Moreover, it is known that the presence of radiation defects yields a smaller critical thickness, or in other words, suppressed microstructural size effects [13,25–27]. Radiation defects not only increase the strength of polycrystalline materials, but also the presence of many radiation defects and their small size have been shown to create a small internal length scale in materials [13,27]. Furthermore, Kohno et al. observed that JFMS (9% Cr) F/M steel size effects were still apparent with light neutron irradiation on the order of mdpa but were diminished after neutron irradiation on the order of 10s of dpa [25].

Looking at the unirradiated SS-J geometry HT-9 studies, it would appear the critical thickness is ~200 μm, however the lath size of F/M steels is typically 1–2 μm [14]. This yields roughly 14 laths across the thickness of our thinnest (29 μm) unirradiated samples, implying there should be no thickness effects observed. Thus, the observed changes in unirradiated tensile properties with respect to thickness may help us separate microstructural size effects from sample geometry effects. Although the irradiated data is too limited to make a definitive

conclusion, it is possible the irradiation effects on the tensile properties are not sensitive to the sample geometry effects.

4. Discussion

Despite the limited test matrix in this experiment, the results are useful in comparing to previous data in the literature. Since many high-Cr (9–12% Cr) F/M steels have common features and have been studied alongside HT-9, they will be referred to in this discussion.

F/M steels are candidate in-core structural materials for future nuclear reactors, where it is estimated that the operating temperature ranges from 280 to 650 °C and light irradiation only occurs at the beginning of the operation lifetime [22]. The HT-9 data available in the irradiation temperature range of 373–427 °C showed that the impact of irradiation on tensile properties diminished at temperatures above 400 °C, but there may be enhanced softening characterized by a decrease in YS due to radiation enhanced diffusion [22].

F/M steels are also envisioned for in-reactor but out-of-core applications, where the temperatures and irradiation fluence may be much less than in-core conditions. A concern for nuclear applications of high-Cr F/M steels has been previously identified to be the low-temperature (≤300 °C) embrittlement resulting from radiation hardening [2,22]. The irradiation-induced upshift in DBTT is particularly concerning for nuclear structural materials, where catastrophic failure is not an option, because it can lead to brittle fracture instead of the preferred ductile ("leaking before breaking") fracture mechanism [28].

Due to the primarily in-core applications for HT-9, little data is available for low temperature irradiations and nearly no data is available <1 dpa. Comprehensive low-temperature (≤300 °C) irradiation and room temperature tensile tests ΔYS and % decrease in UE results are shown in Fig. 7 for a variety of high-Cr F/M steels, alongside results from the low-temperature irradiation experiment in this study. The % decrease in UE is calculated as follows:

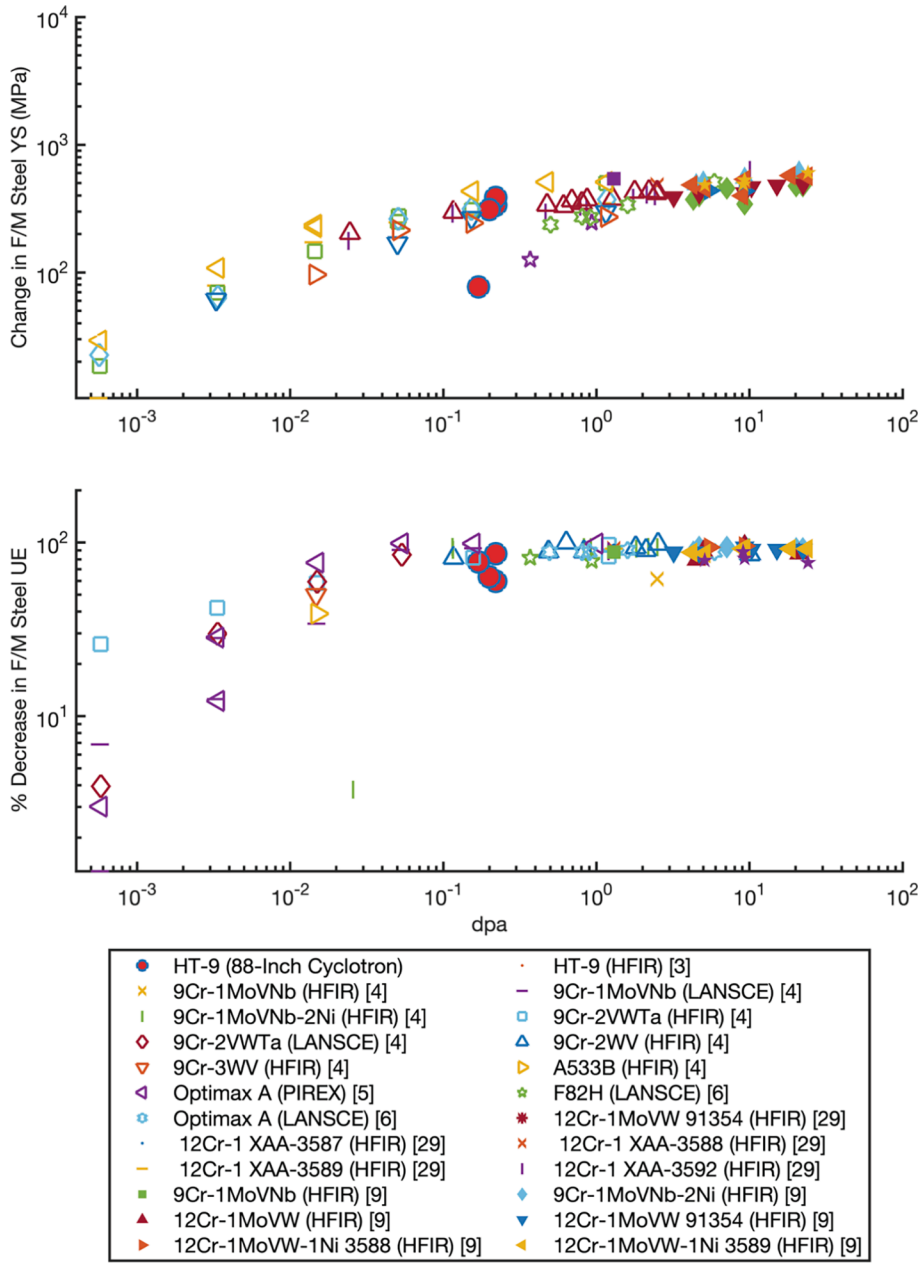

Fig. 7. Change in high-Cr (≥9% Cr) F/M steel YS (ΔYS) and % decrease in UE with respect to dose after various low temperature (≤300 °C) irradiations. The data from this study fits well within the larger body of data obtained in previous works [3–6,9,29].

$$\%\ decrease\ in\ UE\ =\ \frac{UE(0\ dpa) - UE(x\ dpa)}{UE(0\ dpa)}$$

Where $UE(0\ dpa)$ is the reported UE at 0 dpa and $UE(x\ dpa)$ is the reported UE at a specific dpa. The data in Fig. 7 is comprised from a variety of different materials and test parameters described in the Supplementary Table 2.

A general trend is apparent in the ΔYS and % decrease in UE data. Radiation hardening, which is accompanied by an increase in YS and a decrease in UE, begins at the lowest reported doses of 0.0005 dpa and increases sharply until about 0.05 dpa [4], after which hardening continues to steadily increase until saturating around 10 dpa.

The barrier hardening theory was used to explore the radiation-induced increase in yield strength observed in this experiment, assuming the black dot defects are small dislocation loops:

$$\Delta YS = \Delta\sigma_{loop} = M\alpha\mu b\sqrt{Nd}$$

Where $\Delta\sigma_{loop}$ is the hardening contribution from dislocation loops (black dots), M is the Taylor factor, α is the barrier strength, μ is the shear modulus, b is the magnitude of the Burgers vector, N and d are number density and size of dislocations.

Here, the values for constants M, α, and b will be adopted from previous barrier hardening analysis on HT-9, where $M = 3.06$, $\alpha = 0.5$, $\mu = 82$ GPa and $b = 0.249$ nm [24]. From the TEM analysis, Nd was estimated as $1.6 \times 10^{14} \pm 10^{14}$ m^{-2}. As a result, ΔYS estimated by the barrier hardening model is 371 ± 142 MPa, while ΔYS measured for this sample was about 336 MPa. Moreover, ΔYS measured for all samples in other experiments, which were irradiated to similar doses, ranged from 77 to 387 MPa. Thus, the dislocation density estimates and subsequent barrier hardening calculation is within most of the measured ΔYS, especially for the lower bound of the error.

Farrell and Byun previously used models based on barrier hardening theory to describe some of the other body of data shown in Fig. 7, revealing limitations of the model [4]. Farrell and Byun postulated the prominent change in the slope of the general trend around 0.05 dpa coupled with high necking strains indicates a change from the barrier hardening deformation mechanism to dislocation channel deformation [4]. Being our results fall in this slope transition region of the general trend, it is possible that barrier hardening may also be competing with dislocation channeling in our application, hence the lower bound of the dislocation quantification error generally being a better estimation of the ΔYS. However, no search for dislocation channels by TEM was made in this work.

The HT-9 data from this study fits well within the larger body of high-Cr F/M steel data, thereby providing merit for the 0.18–0.22 dpa irradiation and small-scale mechanical testing presented here. This study provides insight on the tensile properties of HT-9 as a function of gauge thickness and dpa. Previously, HT-9 tensile samples have been irradiated in reactors for long durations (e.g. 18 months [12]) and required hot cells for post-irradiation analysis and mechanical testing [1,12]. The use of the 88-Inch Cyclotron alongside miniature SS-J tensile samples can supplement these neutron irradiations by achieving a desired dpa using deuterons. The small tensile sample size and ability to shape the ion beam to the tensile sample gauge length yields less irradiated volume and therefore less radioactive material. This method has potential for rapid turnaround experiments on irradiated tensile sample mechanical testing on a variety of materials and using a variety of ions. However, it is worth noting that dpa achieved in an accelerator (10–30 days) may have a different mechanism than dpa achieved in a reactor, (2–6 months) as the dose rate is known to play an important factor in defect cluster size and number density [30,31].

5. Conclusions

In this work we utilize the LBNL 88-Inch Cyclotron to irradiate SS-J geometry tensile test specimens with ~20–30 MeV deuterons. We also present an approach to quantify tensile properties as a function of gauge thickness, bringing about the potential to bridge length scale gaps. It was found that the low-temperature (<60 °C), low-dose (0.18–0.22 dpa) irradiation caused radiation hardening with an increase the YS of approximately 15–35% and decrease in ductility of about 75%, which is in good agreement with previous low-temperature high-Cr F/M steel experiments. An intermediate ductile/brittle failure mode was observed for all samples. As a result of the irradiation, black dot defects on the order of 6 ± 2 nm and $1.6 \times 10^{14} \pm 10^{14}$ m^{-2} were observed, with the lower error bound yielding most reasonable ΔYS approximations by barrier hardening theory. Additionally, sample geometry effects on tensile properties were observed ~200 μm gauge thickness for unirradiated samples. Future work should be conducted to confirm if these geometric effects are diminished by the 0.18–0.22 dpa irradiation. We have shown that the Cyclotron, coupled with benchtop tensile testing of radioactive samples, enables rapid-turnaround mechanical testing of nuclear structural materials.

Declaration of Competing Interest

The authors declare that they have no known competing financial interests or personal relationships that could have appeared to influence the work reported in this paper.

Data availability

Tensile test data has been made available in the Supplementary material. Additional data will be made available upon request.

Acknowledgements

This research was supported by the U.S. Department of Energy Isotope Program, managed by the Office of Science for Isotope R&D and Production, and was carried out under Lawrence Berkeley National Laboratory Contract No. DE-AC02-05CH11231. This material is based upon work supported by the Department of Energy National Nuclear Security Administration through the Nuclear Science and Security Consortium under Award Number(s) DE-NA0003180. This work was also supported by the U.S. Department of Energy, Office of Nuclear Energy under the Nuclear Energy University Program as a part of an Integrated University Program fellowship.

Appendix A. Supplementary data

Supplementary data to this article can be found online at https://doi.org/10.1016/j.nimb.2022.09.001.

References

[1] S.A. Maloy, M.B. Toloczko, K.J. McClellan, T. Romero, Y. Kohno, F.A. Garner, R. J. Kurtz, A. Kimura, The effects of fast reactor irradiation conditions on the tensile properties of two ferritic/martensitic steels, J. Nucl. Mater. 356 (2006) 62–69, https://doi.org/10.1016/j.jnucmat.2006.05.024.

[2] Y. Chen, Irradiation effects of HT-9 martensitic steel, Nucl. Eng. Technol. 45 (2013) 311–322, https://doi.org/10.5516/NET.07.2013.706.

[3] A.F. Rowcliffe, J.P. Robertson, R.L. Klueh, K. Shiba, D.J. Alexander, M. L. Grossbeck, S. Jitsukawa, Fracture toughness and tensile behavior of ferritic-martensitic steels irradiated at low temperatures, J. Nucl. Mater. 258–263 (1998) 1275–1279, https://doi.org/10.1016/S0022-3115(98)00163-9.

[4] K. Farrell, T.S. Byun, Tensile properties of ferritic/martensitic steels irradiated in HFIR, and comparison with spallation irradiation data, J. Nucl. Mater. 318 (2003) 274–282, https://doi.org/10.1016/S0022-3115(03)00102-8.

[5] N. Baluc, R. Schäublin, C. Bailat, F. Paschoud, M. Victoria, Mechanical properties and microstructure of the OPTIMAX series of low activation ferritic-martensitic steels, J. Nucl. Mater. 283–287 (2000) 731–735, https://doi.org/10.1016/S0022-3115(00)00282-8.

[6] Y. Dai, S.A. Maloy, G.S. Bauer, W.F. Sommer, Mechanical properties and microstructure in low-activation martensitic steels F82H and Optimax after 800-MeV proton irradiation, J. Nucl. Mater. 283 (2000) 513–517, https://doi.org/10.1016/S0022-3115(00)00267-1.

[7] R.L. Klueh, J.M. Vitek, Tensile behavior of irradiated 12Cr-1MoVW steel, J. Nucl. Mater. 137 (1985) 44–50, https://doi.org/10.1016/0022-3115(85)90047-9.
[8] R.L. Klueh, J.M. Vitek, Postirradiation tensile behavior of Nickel-dopes ferritic Steels, J. Nucl. Mater. 150 (1987) 272–280. https://doi.org/https://doi.org/10.1016/0022-3115(87)90004-3.
[9] R.L. Klueh, J.M. Vitek, Fluence and helium effects on the tensile properties of ferritic steels at low temperatures, J. Nucl. Mater. 161 (1989) 13–23, https://doi.org/10.1016/0022-3115(89)90457-1.
[10] P. Hosemann, Small-scale mechanical testing on nuclear materials: bridging the experimental length-scale gap, Scr. Mater. 143 (2018) 161–168, https://doi.org/10.1016/j.scriptamat.2017.04.026.
[11] T. Ajantiwalay, L. Nagel, S. Maloy, K. Hattar, J.J. Mecholsky, A. Aitkaliyeva, Investigation of hardening mechanisms and size effects in proton-irradiated HT-9 steels, J. Nucl. Mater. 548 (2021) 152866.
[12] P. Hosemann, Y. Dai, E. Stergar, H. Leitner, E. Olivas, A.T. Nelson, S.A. Maloy, Large and Small Scale Materials Testing of HT-9 Irradiated in the STIP Irradiation Program, Exp. Mech. 51 (2011) 1095–1102, https://doi.org/10.1007/s11340-010-9419-2.
[13] P. Hosemann, C. Shin, D. Kiener, Small scale mechanical testing of irradiated materials, J. Mater. Res. 30 (2015) 1231–1245, https://doi.org/10.1557/jmr.2015.26.
[14] A. Dong, H. Vo, E. Olivas, C. Hardie, P. Hosemann, S. Maloy, Micro-Mesoscale Mechanical Testing of 304SS, HT-9, and CuCrZr, Unpublished Manuscript, (2022).
[15] M. Kireeff Covo, R.A. Albright, B.F. Ninemire, M.B. Johnson, A. Hodgkinson, T. Loew, J.Y. Benitez, D.S. Todd, D.Z. Xie, T. Perry, L. Phair, L.A. Bernstein, J. Bevins, J.A. Brown, B.L. Goldblum, M. Harasty, K.P. Harrig, T.A. Laplace, E. F. Matthews, A. Bushmaker, D. Walker, V. Oklejas, A.R. Hopkins, D.L. Bleuel, J. Chen, S.B. Cronin, The 88-Inch Cyclotron: A one-stop facility for electronics radiation and detector testing, Meas. J. Int. Meas. Confed. 127 (2018) 580–587, https://doi.org/10.1016/j.measurement.2017.10.018.
[16] J.R. Cooper, L. Bernstein, M.A. McMahan, J. Powell, D. Wutte, L. Ahle, N. Benczer-Koller, D. Dashdorj, G. Kumbartzki, T.J. Mertzimekis, A. Schiller, C. Silver, M. J. Taylor, Production of a 76Kr radioactive ion beam using a batch mode method, Nucl. Instruments Methods Phys. Res. Sect. A Accel. Spectrometers, Detect. Assoc. Equip. 533 (2004) 287–294, https://doi.org/10.1016/j.nima.2004.06.151.
[17] A. Trkov, P.J. Griffin, S.P. Simakov, L.R. Greenwood, K.I. Zolotarev, R. Capote, D. L. Aldama, V. Chechev, C. Destouches, A.C. Kahler, C. Konno, M. Koštál, M. Majerle, E. Malambu, M. Ohta, V.G. Pronyaev, V. Radulović, S. Sato, M. Schulc, E. Šimečková, I. Vavtar, J. Wagemans, M. White, H. Yashima, IRDFF-II: A New Neutron Metrology Library, Nucl. Data Sheets. 163 (2020) 1–108, https://doi.org/10.1016/j.nds.2019.12.001.
[18] J.F. Ziegler, J.P. Biersack, M.D. Ziegler, The Stopping and Range of Ions in Matter, 7th ed., SRIM Co., Chester, MD, 2008.
[19] J.T. Morrell, A.S. Voyles, M.S. Basunia, J.C. Batchelder, E.F. Matthews, L. A. Bernstein, Measurement of 139La(p, x) cross sections from 35–60 MeV by stacked-target activation, Eur. Phys. J. A. 56 (2020), https://doi.org/10.1140/epja/s10050-019-00010-0.
[20] H. Junde, H. Su, Y. Dong, Nuclear Data Sheets for A = 56, Nucl. Data Sheets. 112 (2011) 1513–1645, https://doi.org/10.1016/j.nds.2011.04.004.
[21] Brookhaven National Laboratory, B. Pritychenko, A. Sonzogni, NNDC Q-value Calculator (Q-Calc), (n.d.). https://www.nndc.bnl.gov/qcalc.
[22] R.L. Klueh, Elevated temperature ferritic and martensitic steels and their application to future nuclear reactors, Int. Mater. Rev. 50 (2005) 287–310, https://doi.org/10.1179/174328005X41140.
[23] C. Zheng, S. Maloy, D. Kaoumi, Effect of dose on irradiation-induced loop density and Burgers vector in ion-irradiated ferritic/martensitic steel HT9, Philos. Mag. 98 (2018) 2440–2456, https://doi.org/10.1080/14786435.2018.1490825.
[24] H. Yan, X. Liu, L. He, J. Stubbins, Phase stability and microstructural evolution in neutron-irradiated ferritic-martensitic steel HT9, J. Nucl. Mater. 557 (2021), 153252, https://doi.org/10.1016/j.jnucmat.2021.153252.
[25] Y. Kohno, A. Kohyama, M.L. Hamilton, T. Hirose, Y. Katoh, F.A. Garner, Specimen size effects on the tensile properties of JPCA and JFMS, J. Nucl. Mater. 283–287 (2000) 1014–1017, https://doi.org/10.1016/S0022-3115(00)00245-2.
[26] A. Kohyama, K. Hamada, H. Matsui, Specimen size effects on tensile properties of neutron-irradiated steels, J. Nucl. Mater. 179–181 (1991) 417–420, https://doi.org/10.1016/0022-3115(91)90113-L.
[27] E. Azrt, Size effects in materials due to microstructural and dimensinal constraints: A comparative review, Acta Mater. 46 (1998) 5611–5626. https://doi.org/https://doi.org/10.1016/S1359-6454(98)00231-6.
[28] M.E. Launey, R.O. Ritchie, On the fracture toughness of advanced materials, Adv. Mater. 21 (2009) 2103–2110, https://doi.org/10.1002/adma.200803322.
[29] R.L. Klueh, J.M. Vitek, M.L. Grossbeck, Effect of low-temperature irradiation with (n,alpha) Helium production on tensile properties of 12-Cr-1MoVW-type steels, J. Nucl. Mater. 103 & 104 (1981) 887–892. https://doi.org/https://doi.org/10.1016/0022-3115(82)90712-7.
[30] S. Jepeal, L. Snead, Z. Hartwig, Intermediate energy proton irradiation: rapid, high-fidelity materials testing for fusion and fission energy systems, Eprint ArXiv: 2009.00048 [Preprint]. (2020). http://arxiv.org/abs/2009.00048.
[31] G.S. Was, Z. Jiao, E. Getto, K. Sun, A.M. Monterrosa, S.A. Maloy, O. Anderoglu, B. H. Sencer, M. Hackett, Emulation of reactor irradiation damage using ion beams, Scr. Mater. 88 (2014) 33–36, https://doi.org/10.1016/j.scriptamat.2014.06.003.